Clinical Applications of Diffusion Tensor Imaging

Tammie L. S. Benzinger, M.D., Ph.D.[1]; Robert C. McKinstry III, M.D., PhD.[2]; Chin-I Chen, M.D[1]; Agus Priatna, Ph.D.[3]

[1]*Mallinckrodt Institute of Radiology, Washington University School of Medicine, St Louis, Missouri, USA*
[2]*St. Louis Children Hospital, Mallinckrodt Institute of Radiology, Washington University School of Medicine, St Louis, Missouri, USA*
[3]*Siemens Medical Solutions, Malvern, PA, USA*

Introduction

Diffusion tensor imaging (DTI) is an emerging method for clinical neuroradiology. DTI allows for quantitative evaluation of the rate and direction of water motion within a voxel. In the brain, the axons of neurons form fiber tracts which impose directionality (anisotropy) on measurements of water diffusion. The aggregate diffusion of water within these tracts is quantified at each point by the diffusion tensor (D) [Stejskal and Tanner, 1965]. Multiple parameters can be derived from the diffusion tensor, including the „trace", Tr(D)= 1 + 2 + 3 = 3 × ADC (apparent diffusion coefficient), the relative anisotropy (RA, defined as the standard deviation of the three eigenvalues, normalized by the ADC), and the fractional anisotropy (FA, which is the standard deviation of the three eigenvalues normalized to the magnitude of the diffusion tensor). These secondary parameters are independent of the frame of reference and are very sensitive to white matter pathology [Alexander et al., 2007; Melhem et al., 2002].

Until recently, DTI required extensive off-line calculations to generate the tensor (D) and related parameter maps. However, using the current DTI packages available on the Tim (Total imaging matrix) platforms, DTI can now be performed as part of a routine clinical brain MRI, with Inline calculation of the D, ADC, and FA, and rapid off-line calculation of additional parameter maps as needed. We have developed a 25-direction DTI protocol with 25 b-values which can be run with isotropic 1 mm voxels at 3 Tesla in 4 minutes. We now include this as part of the standard imaging routine for pediatric and adult brain MRIs at St. Louis Children's Hospital and Washington University Medical Center.

Method

Imaging was performed at 3 Tesla MAGNETOM Trio, A Tim System or 1.5 Tesla MAGNETOM Symphony, A Tim System with Quantum gradient system using 12-channel Head Matrix coils. A single shot spin-echo echo planar imaging (EPI) was used for DTI acquisition at the Tim Trio with the following parameters: 60 slices without a gap, FoV = 190 mm, phase FoV = 100 %, slice thickness = 2 mm, base resolution = 96, phase resolution = 100 (that makes voxel size = 2 x 2 x 2 mm), phase partial Fourier = 6/8, TR = 9900 msec, TE = 102 msec, average = 1, b-value = 1400 sec/mm^2, bandwidth = 1080 Hz, EPI factor = 96, echo spacing = 1 msec. A similar protocol was setup for the Tim Symphony with 2.5 x 2.5 x 2.5 mm isotropic voxel. Average ADC map, trace weighted map, FA map, and tensor data were created inline. Post-processing was performed with Neuro 3D application package. The package has the capability of processing directional color encoded fractional anisotropy map (blue = SI direction, green = AP direction, and red = RL direction), tensor map, aligned tensor and anatomy data, aligned tensor and fractional anisotropy data, texture diffusion that maps the overall fiber tracts within the slices, and tractography.

Clinical cases

The following cases are some of the examples of the clinical applications of diffusion tensor imaging in pediatrics and adults which we have encountered in the course of routine clinical practice.

Case 1: Septo-optic dysplasia

A 14-year-old boy was admitted to the hospital with severe, chronic headaches. MRI shows absence of the septum pellucidum is consistent with his clinical diagnosis of septo-optic dysplasia. Moderate hydrocephalus and thinning of the corpus callosum were found. DTI show marked diminution, with significant reduction in the visual fiber tracts of the optic radiations but with persistent anisotropy (Fig. 1). These findings are concordant with his clinical presentation of intact visual function and are also in accordance with reports in the literature [Polizzi et al., 2006; Schoth et al., 2004]. Septo-optic dysplasia consists of a heterogenous deficits of midline brain structures which include absence or dysplasia of septum pellucidum, optic nerve and pituitary-hypothalamic dysfunction. In addition, the lesions may associate cerebral development malformations such as schizencephaly and polymicrogyria. A HESX1 gene mutation has been identified in familial septo-optica dysplasia. Clinical manifestations include diminished visual acuity, color blindness, nystagmus, microphthalmia, mental retardation, and endocrine disturbance.

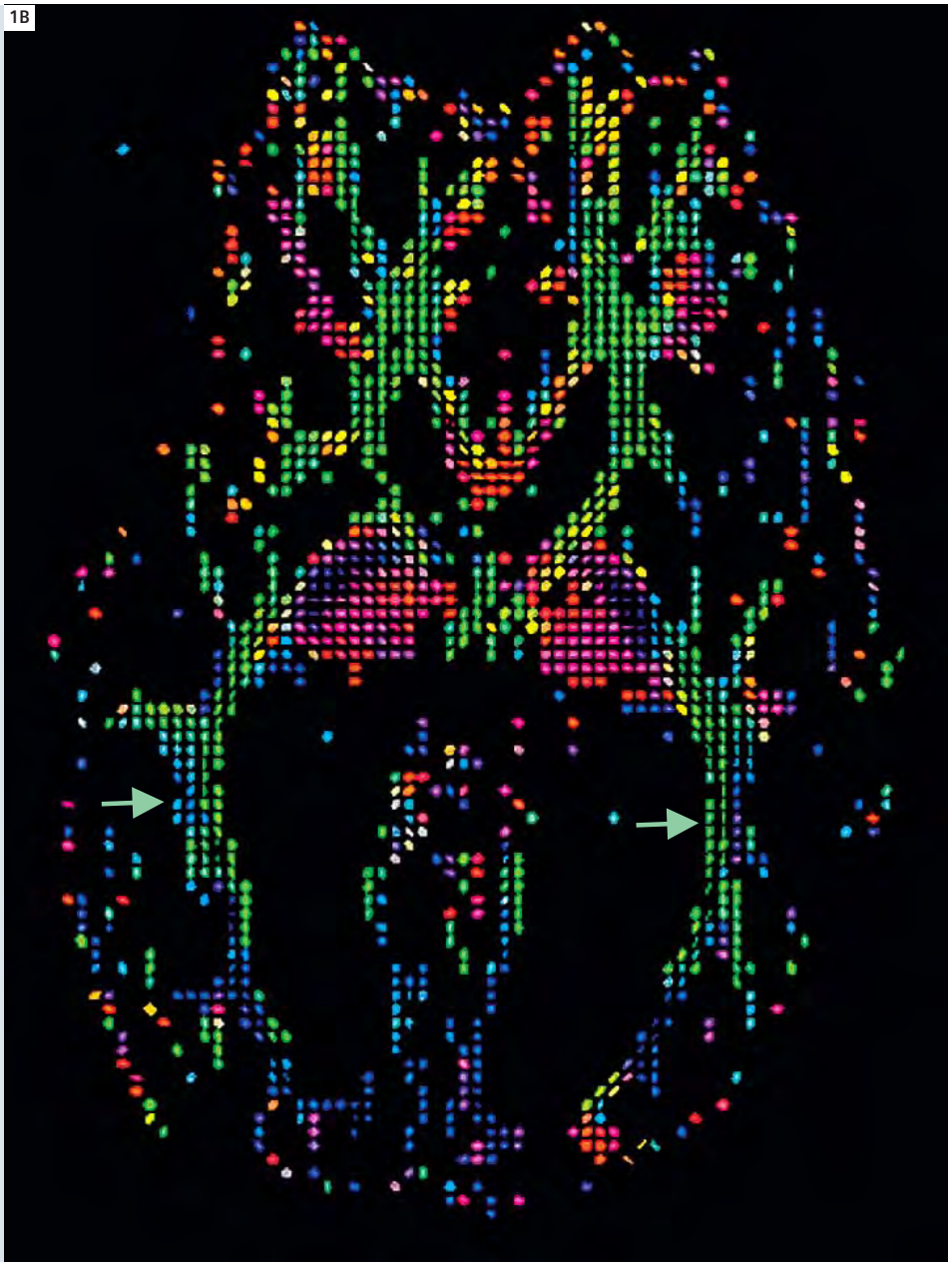

1 Septo-optic dysplasia. MR examinations were performed at 3T MAGNETOM Trio, A Tim System: **(A)** T1-weighted (MPRAGE) anatomic image demonstrating enlargement of the ventricles and absence of the septum pellucidum (arrow). **(B)** Tensor diagram computed from a 4 minute DTI scan performed with isotropic 2 mm voxels at 3 Tesla. The shape and color of the ellipsoids corresponds to the orientation of the white matter tract (anterior-posterior is green, transverse is red, and cranio-caudal is blue). The optic radiations (arrowheads) adjacent to the lateral ventricles are thin but intact.

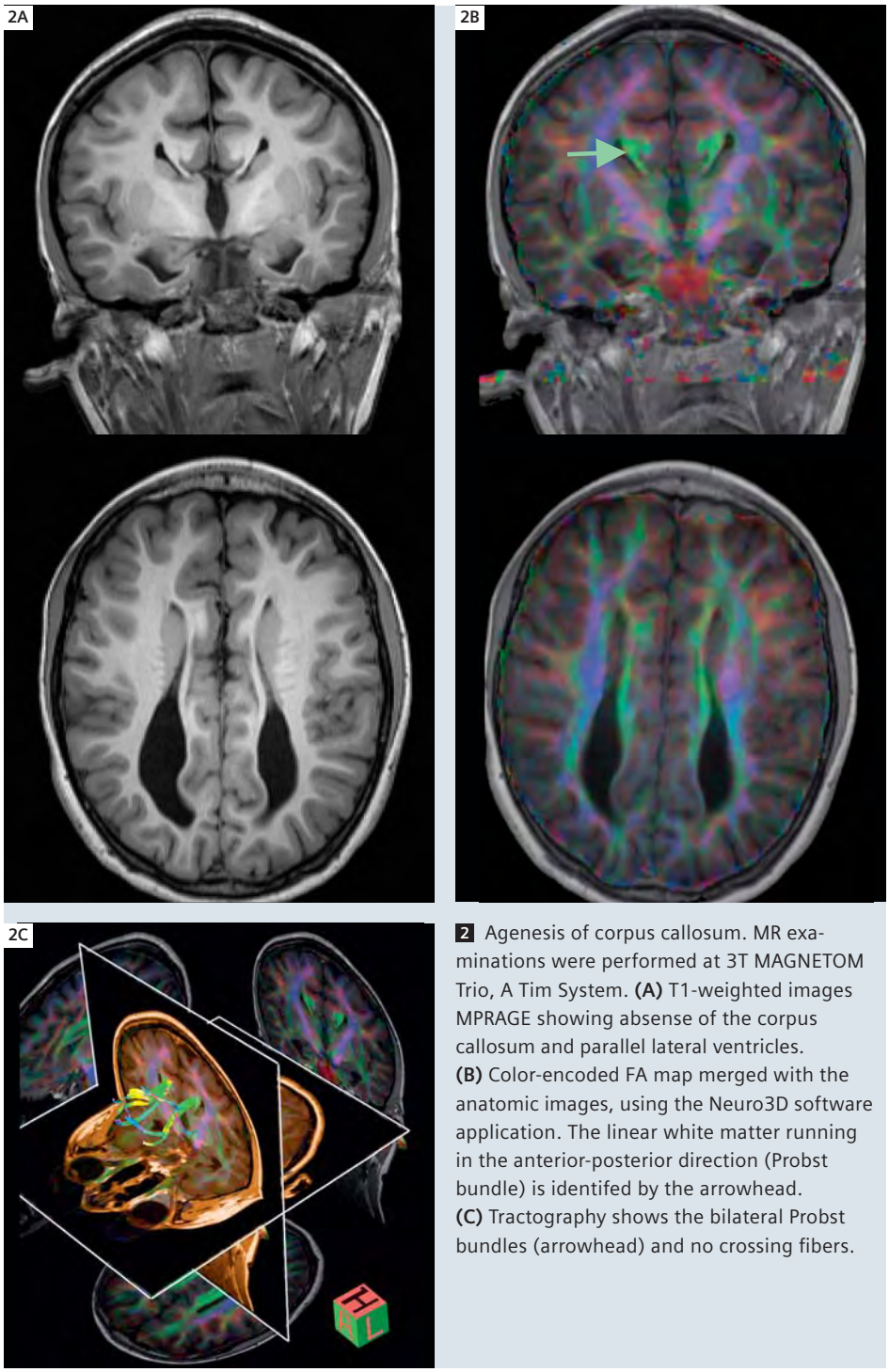

2 Agenesis of corpus callosum. MR examinations were performed at 3T MAGNETOM Trio, A Tim System. **(A)** T1-weighted images MPRAGE showing absense of the corpus callosum and parallel lateral ventricles. **(B)** Color-encoded FA map merged with the anatomic images, using the Neuro3D software application. The linear white matter running in the anterior-posterior direction (Probst bundle) is identifed by the arrowhead. **(C)** Tractography shows the bilateral Probst bundles (arrowhead) and no crossing fibers.

Case 2: Agenesis of corpus callosum

A 9-year-old girl was diagnosed with developmental delay and intractable seizures. MRI shows colpocephaly, parallel lateral ventricles, and agenesis of the corpus callosum. DTI shows no crossing fibers in the expected region of the corpus callosum (Fig. 2). With tractography, the orientation of the parallel Probst bundles are clearly identified. Tractography has recently been described as a useful imaging approach to callosal agenesis and dysgenesis [Tovar-Moll, 2007]. Agenesis of corpus callosum is a failure to develop the large bundle of fibers that connect the cerebral hemispheres. The complex disorder can result from any one of the multiple steps of callosal development, such as cellular proliferation and migration, axonal growth or glial patterning at the midline. Its subjacent mechanisms are still unknown. Patients can show variable presentations ranging from no symptoms to severe cognitive impairment [Paul et al., 2007].

Case 3: Schizencephaly

A 4-year-old girl has a past history of seizures. MRI (Fig. 3) shows a major malformation of cortical development involving the left motor strip, dorsal lateral premotor region, frontal operculum, frontal polar region, orbital frontal and lateral frontal regions, parietal operculum, and posterior temporal lobe. An associated left-sided schizencephaly is identified. The left lateral ventricle is mildly dilated. There is abnormal configuration of the central sulcus on the left. DTI shows diminished anisotropy of the underlying white matter region in subjacent to the malformation of cortical development [Eriksson et al., 2001; Trivedi, et al., 2006]. Schizencephaly presents a cleft in the cerebral cortex unilaterally or bilaterally, usually located in the frontal area. Associated septum pellucidum deficits are often found, suggesting that schizencephaly may share similar genetic mechanisms with septo-optic dysplasia. Mutation in the EMX2 gene can lead to schizencephaly. Clinical symptoms include seizures and mental impairment [Tanaka et al., 2000].

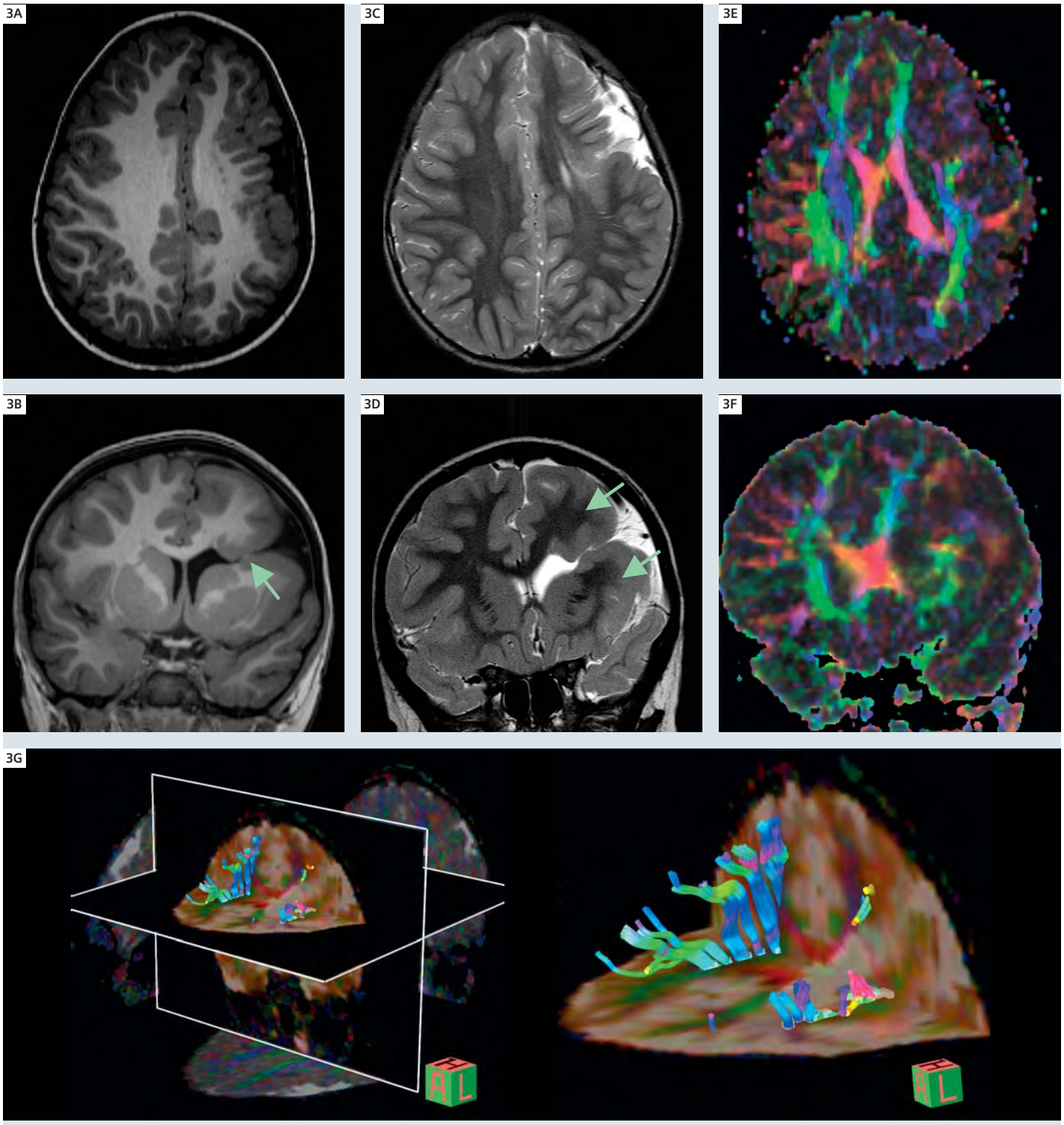

3 Schizencephaly. MR examinations were performed at 3T MAGNETOM Trio, A Tim System. T1 **(A, B)** and T2-weighted **(C, D)** transverse **(A,C)** and coronal images **(B, D)** demonstrating a large schizencephalic cleft in the left cerebral hemisphere (arrow). Accompanying this is an extensive malformation of cortical development (arrowheads). Although the white matter underlying the abnormal cortex appears normal on the clinical T1 and T2-weighted images, when the directional encoded FA map is superimposed on the anatomic images **(E, F)** there is complete loss of the normal (green and red) anisotropy in this white matter. **(G)** Tractography images show the tortuous fibers which do not cross the schizencephalic cleft.

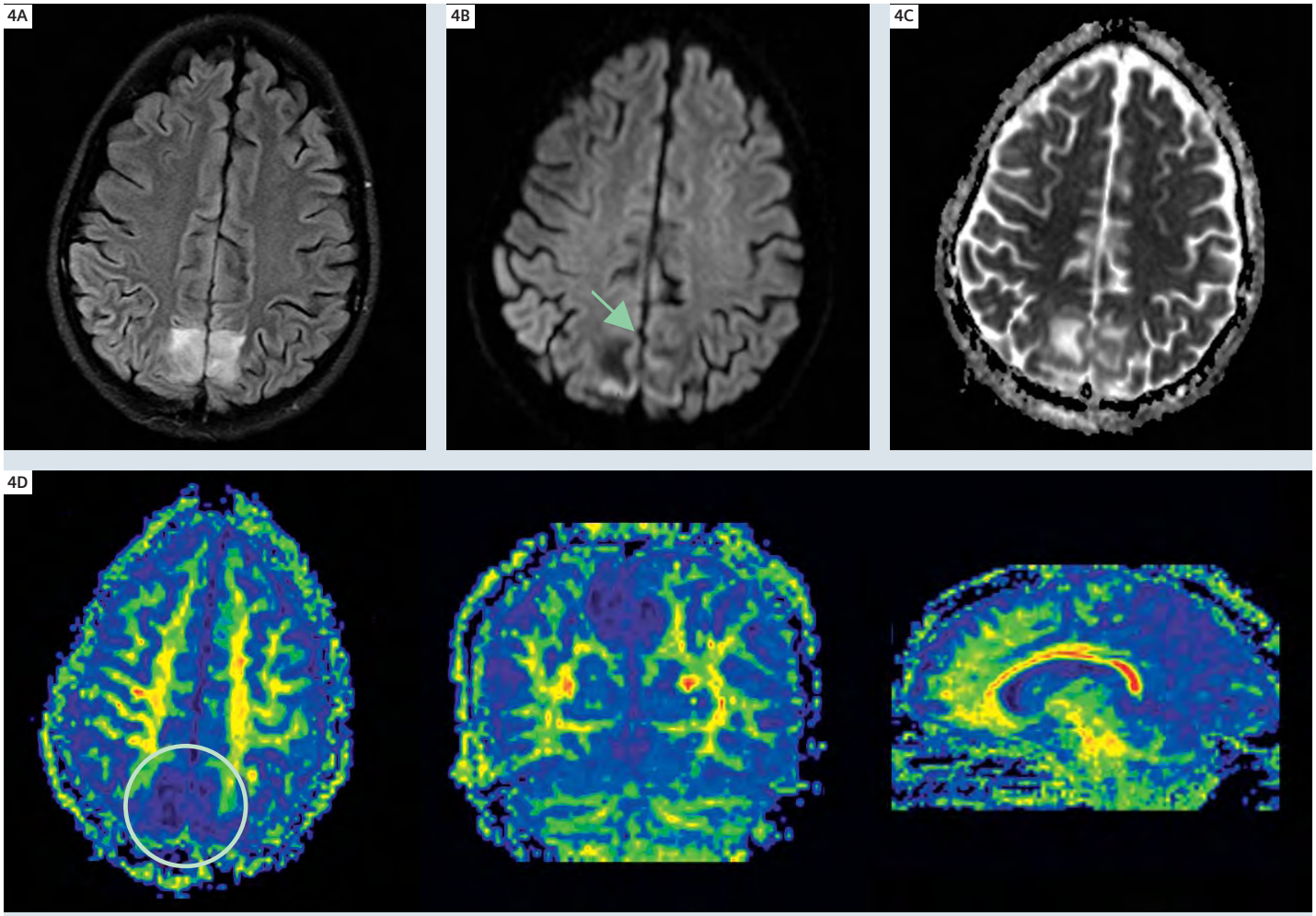

4 Reversible Posterior Leukoencepalopathy Syndrome (RPLS). MR examinations were performed at 3T MAGNETOM Trio, A Tim System: **(A)**, **(B)**, and **(C)** are the DarkFluid T2-weighted TSE, b = 0 image, and ADC map shows the area of restricted diffusion. **(D)** Fractional anisotropy, reformatted in transversal, coronal, and sagittal orientations shows loss of anisotropy in the right parietal lobe extending beyond the areas of T2 hyperintensity.

Case 4: Reversible Posterior Leukoencepalopathy Syndrome (RPLS)

A 13-year-old girl who with a past medical history of hypertension and end stage renal disease was transferred to pediatric ICU because of hypertensive seizure. MRI shows bilateral posterior parietal-occipital areas of T2 hyperintensity, with a focal area of reduced diffusion in the right parietal lobe. The FA parameter map derived from DTI demonstrates an area of abnormal anisotropy in the right parietal lobe which extends beyond the area of T2 hyperintensity (Fig. 4). Although restricted diffusion can has been reported in RPLS, the FA changes in the surrounding white matter have not previously been examined. Incorporating DTI into the routine clinical protocol will allow for larger research studies to be generated to further evaluate this finding [Mukherjee et al., 2001]. RPLS is a clinicoradiological entity which appears as reversible white matter edema predominantly involving the parietal and occipital lobes. The syndrome has been associated with a spectrum of disorders, including hypertensive encephalopathy, eclampsia, thrombotic thrombocytopenic purpura, acute renal failure, hemolytic-uremic syndrome, acute intermittent porphyria, and immunosuppressive drugs. The eitiology of RPLS is believed to be due to a breakdown of the blood-brain barrier with transudation of fluid and protein into the extravascular space resulting in cerebral edema [Min et al., 2006; Doelken et al., 2007].

Case 5: Pediatric demyelination

A 17-year-old boy was admitted with acute onset of headache, double vision, gait instability and nausea. MRI shows abnormalities on the right internal capsule, right periventricular, right mid brain, and right cerebellum. Eigenvalues of DTI show increased radial diffusivity but normal axial diffusivity at the lesion site, which is consistent with demyelinating disease (Fig. 5) and suggests myelin loss without axonal injury. As predicted by the DTI analysis, the child had an almost complete clinical recovery within a few weeks [Mukherjee et al., 2001; Song et al., 2002]. The central nerve system inflammatory demyelinating disorders of childhood include both self-limited (monophasic or recurrent acute disseminated encephalomyelitis ADEM, neuromyelitis optica NMO, clinical isolated syndrome CIS) and life-long (multiple sclerosis) conditions, which can be indistinguishable at the time of initial presentation. ADEM is an acute or subacute white matter disease of brain and spinal cord that often follows a viral illness or vaccination. MS results in recurrent episode and is more likely to develop significant disability [Inglese et al., 2002; Krupp, et al., 2007].

5A

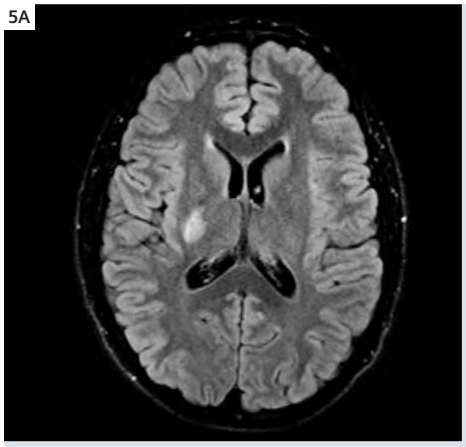

5B

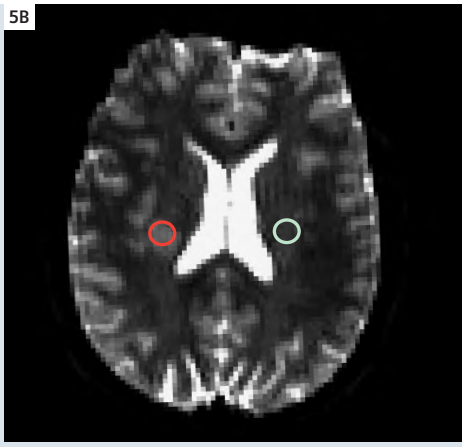

5C

ID	FA Mean Size / Min / Max	FA SDev	ADC Mean Size / Min / Max	ADC SDev	TraceW Mean Size / Min / Max	TraceW SDev	b0 Mean Size / Min / Max	b0 SDev
1	454.5 2 / 421 / 488	33.5	956.0 2 / 930 / 982	26.0	247.0 2 / 247 / 247	0.0	642.5 2 / 626 / 659	16.5
2	650.5 2 / 621 / 680	29.5	663.0 2 / 650 / 676	13.0	187.0 2 / 184 / 190	3.0	363.0 2 / 352 / 374	11.0

ID	Mean Size / Min / Max	SDev	Mean Size / Min / Max	SDev	Mean Size / Min / Max	SDev	Mean Size / Min / Max	SDev
1	1534.5 2 / 1505 / 1564	29.5	1062.0 2 / 1016 / 1108	46.0	206.0 2 / 198 / 214	8.0	624.5 2 / 620 / 629	4.5
2	1462.3 3 / 1392 / 1506	50.2	446.7 3 / 307 / 521	98.3	209.3 3 / 207 / 211	1.7	78.7 3 / 53 / 106	21.7

5D

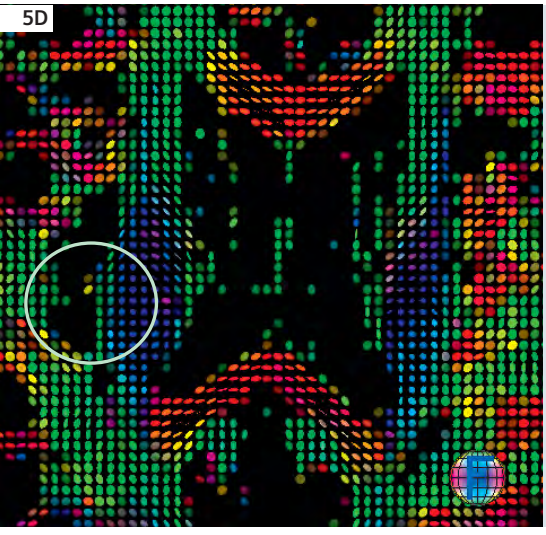

5E

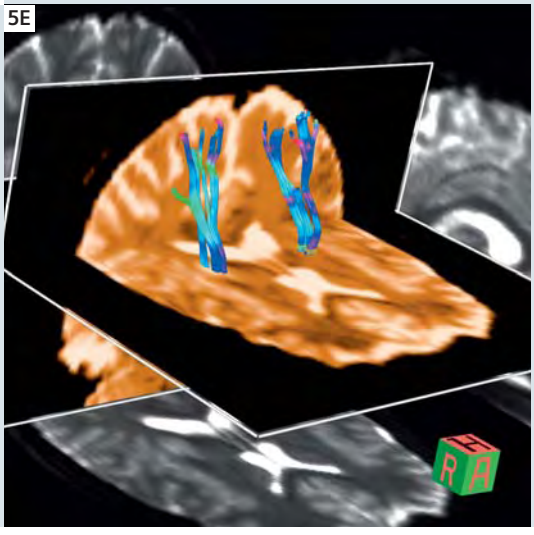

5 Pediatric demyelination. MR examinations were performed at 3T MAGNETOM Trio, A Tim System: **(A)** DarkFluid T2-weighted image shows abnormality on the right side of the brain. **(B)** DTI acquisition was acquired at 2 mm isotropic resolution. Regions of interest at normal (green) and lesion (red) sites were drawn at the diffusion image with b = 0. **(C)** Measurement shows increase in E2 and E3 (radial diffusivity) in the lesion site while the E1 (axial diffusivity) are the same bilaterally. **(D)** Tensor image shows the abnormality in the lesion site. **(E)** Tractography images show that the tracts in the lesion remain intact.

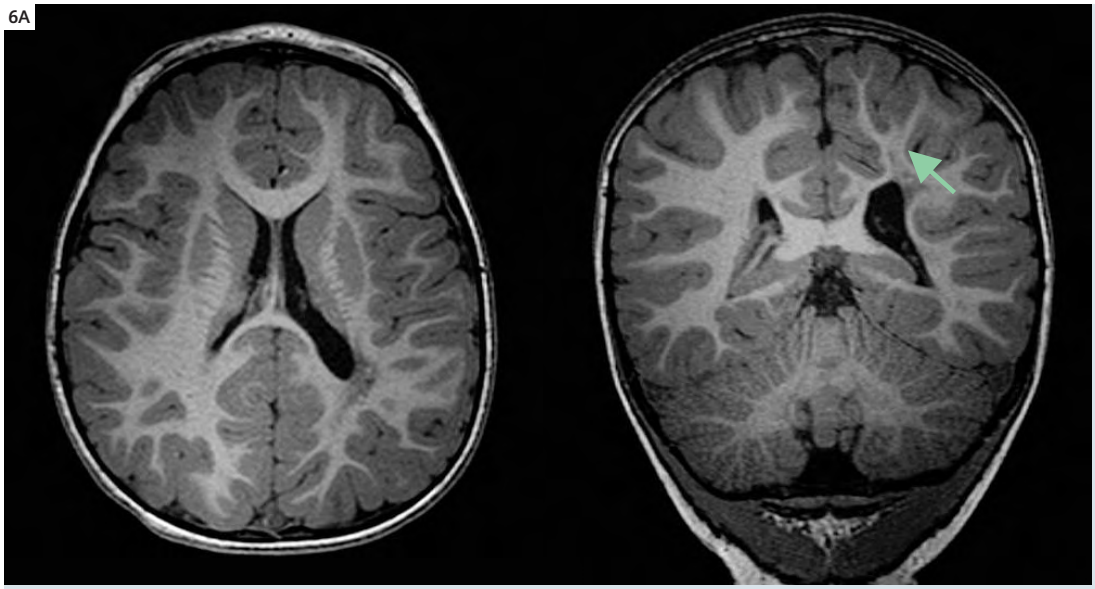

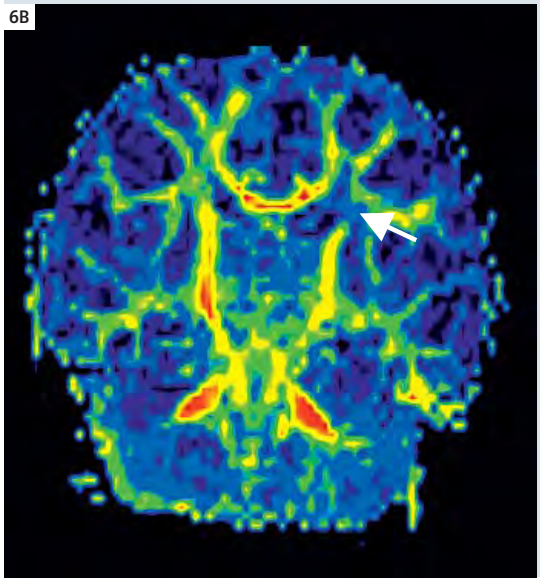

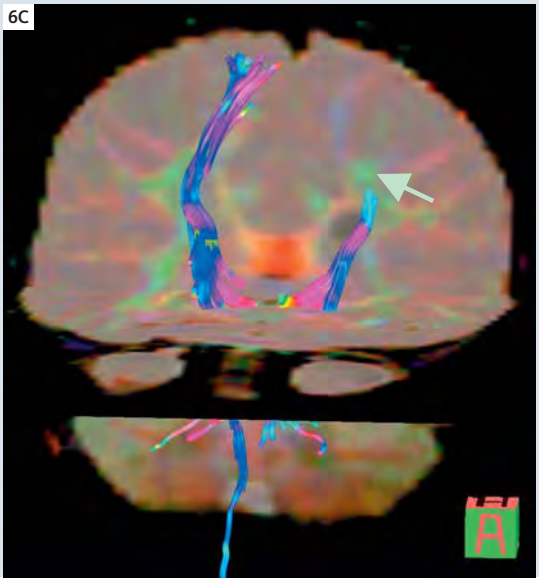

6 Periventricular Leukomalacia. MR examinations were performed at 3T MAGNETOM Trio, A Tim System:
(A) Isotropic 1 mm MPRAGE, reformatted to the transversal and coronal orientations showing the abnormality involving left peritrigonal white matter (arrowhead), with thinning of the white matter and ex-vacuo dilatation of the lateral ventricle.
(B) Coronal reformatted fractional anisotropy shows focal loss of anisotropy at the same location in the left periventricular white matter.
(C) Tractography shows interrupted fibers of the left corticospinal tract at the lesion site, explaining the patient's right hemiparesis.

Case 6: Periventricular leukomalacia

A 2-year-old girl has history of meningitis, right hemiplegia, and difficulty with balance. Her degree of disability was not immediately concurrent with the very minimal findings on the routine clinical MRI which shows mildly decreased T1 and focal increased T2 signal involving left peritrigonal white matter, and mild thinning of the posterior body of the corpus callosum. However, DTI shows the T2 hyperintense lesion corresponds to focal reduced anisotropy centered in a critical location in the left corticospinal tract. Tractography demonstrates interruption of the left corticospinal tract at this level, which is concurrent with the clinical finding of right hemiplegia (Fig. 6). Periventricular leukomalacia refers to the most common damage of the immature cerebral white matter in the perinatal period. It is related to the susceptibility of the periventricular white matter to focal ischemic, infective, or inflammatory destructive processes of neonates. Pathologically, it is characterized by focal necrosis in the periventricular region and diffuse reactive gliosis in the surrounding white matter [Folkerth, 2006; Nagae, 2006; Ward et al., 2006].

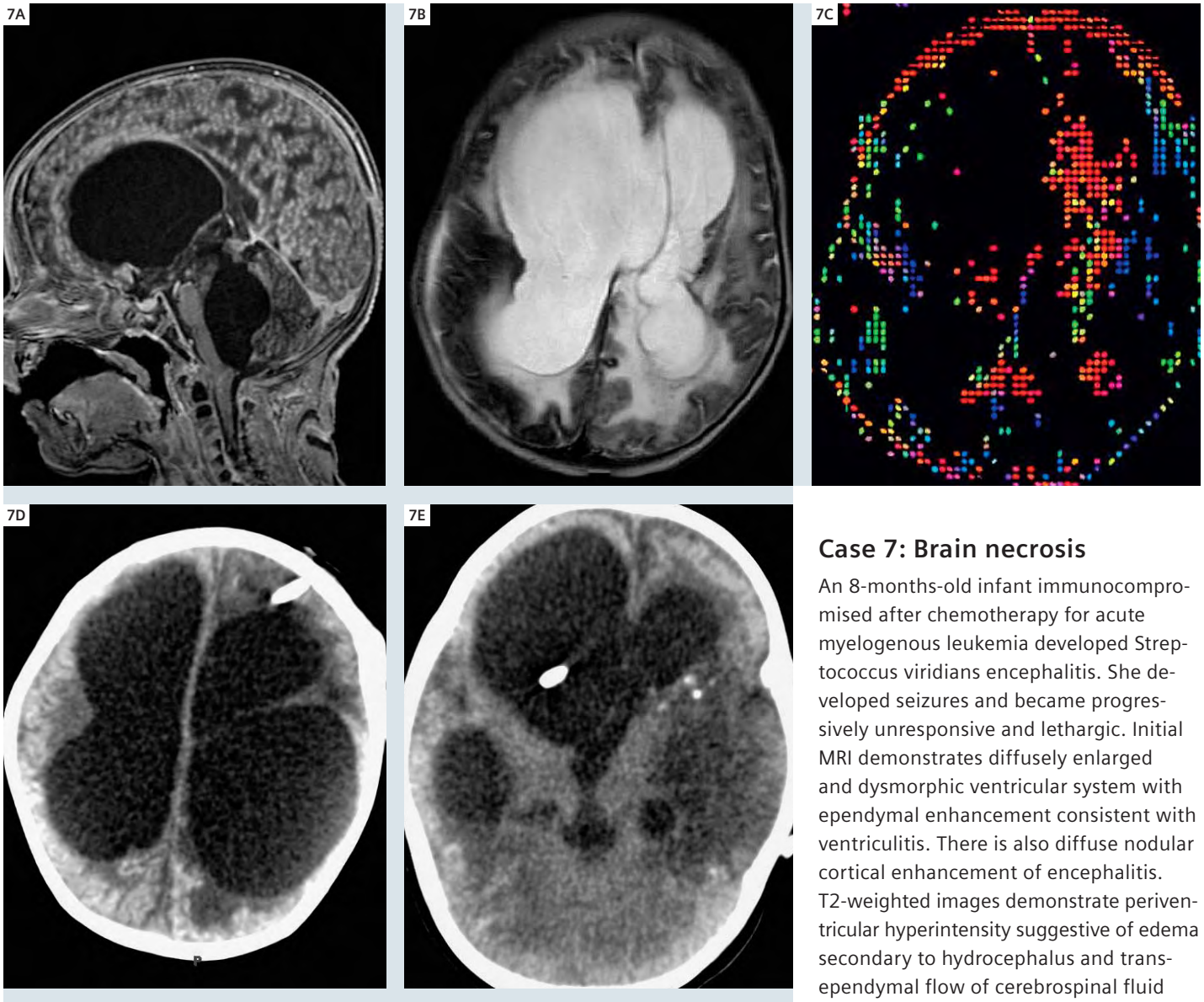

7 Brain necrosis. MR examinations were performed at 3T MAGNETOM Trio, A Tim System: **(A)** Post-contrast SE T1-weighted sagittal images of the brain demonstrate severe ventriculomegaly, periventricular ependymal enhancement, and diffuse granular enhancement of the cortex. These findings suggest severe ventriculitis and encephalitis. **(B)** Axial TSE T2-weighted images demonstrating ventriculomegaly and surrounding T2 hyperintensity of the white matter. In the setting of ventriculomegaly, the most common cause of periventricular white matter T2 hyperintensity is transependymal flow of CSF due to hydrocephalus. **(C)** Fractional anisotropy DTI with ellipsoid and color encoding demonstrates complete loss of normal periventricular white matter anisotropy (for comparison, see figure 5D). Inclusion of DTI in this routine clinical protocol thus suggested an alternate diagnosis of diffuse brain necrosis. **(D)** Non-contrast CT obtained 6 weeks after the initial MRI confirms initial imaging finding. Ventricular catheter failed to fully decompress the ventricles. There is loss of periventricular white matter and diffuse cerebral atrophy secondary to brain necrosis.

Case 7: Brain necrosis

An 8-months-old infant immunocompromised after chemotherapy for acute myelogenous leukemia developed Streptococcus viridians encephalitis. She developed seizures and became progressively unresponsive and lethargic. Initial MRI demonstrates diffusely enlarged and dysmorphic ventricular system with ependymal enhancement consistent with ventriculitis. There is also diffuse nodular cortical enhancement of encephalitis. T2-weighted images demonstrate periventricular hyperintensity suggestive of edema secondary to hydrocephalus and transependymal flow of cerebrospinal fluid (CSF). However, DTI demonstrates periventriular loss of anisotropy and near-total destruction of white matter tracts confirming brain necrosis (Fig. 7). This was confirmed by the patient's clinical course and subsequent imaging.

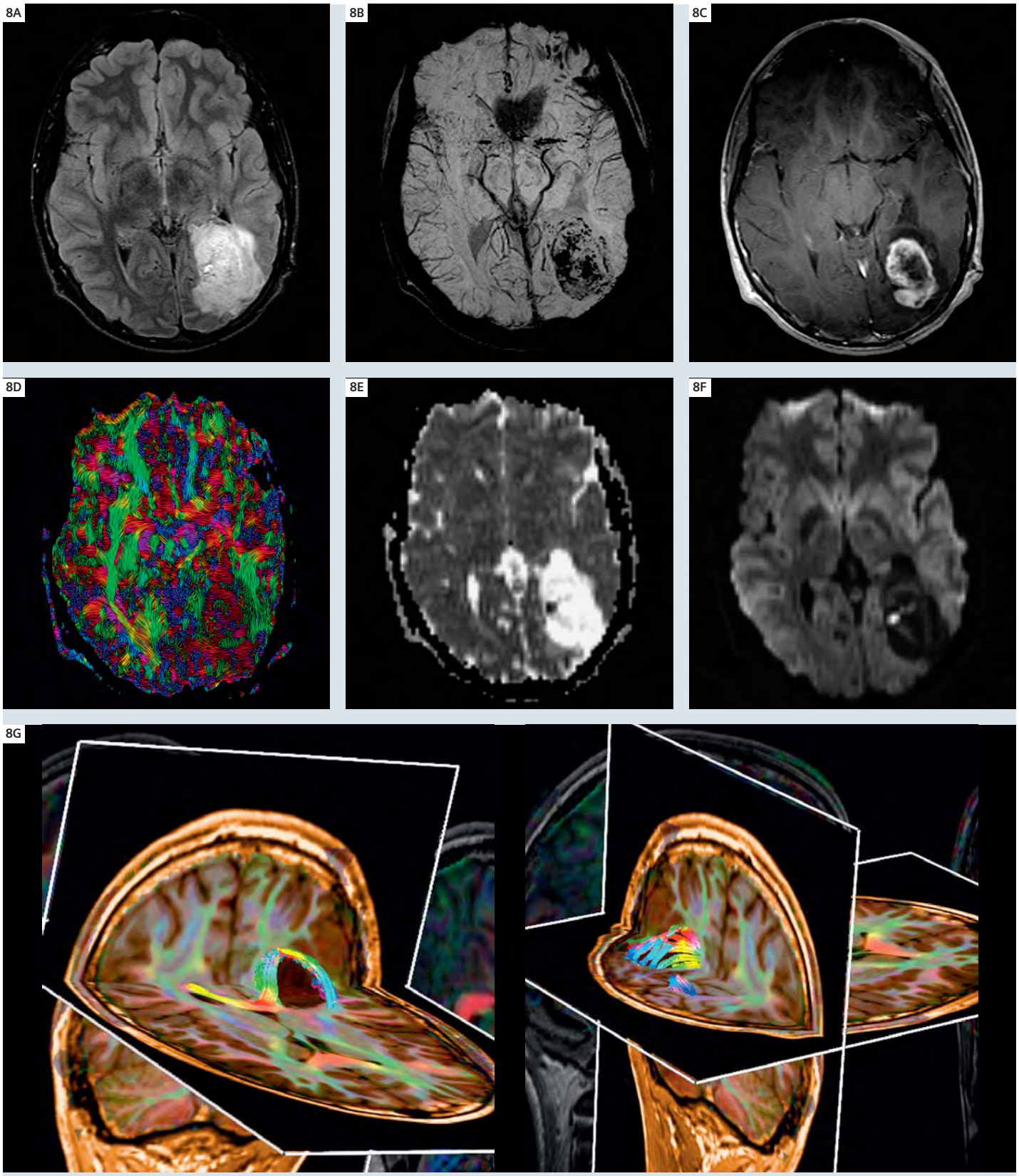

8 DNET tumor. MR examinations were performed at 3T MAGNETOM Trio, A Tim System: **(A)** DarkFluid T2-weighted image demonstrates focal T2 hyperintensity within the left temporooccipital lobe, displacing the trigone of the let lateral ventricle anteriorly. **(B)** Susceptibility weighted imaging (SWI) demonstrates central hemorrhage (signal loss) within the mass. **(C)** Postcontrast T1-weighted image demonstrates the left temporooccipital enhancing mass. **(D)** Texture diffusion showing the possible tracts within the slices. **(E)** and **(F)** are ADC map and trace-weighted images. **(G)** Tractography showing the tracts splitting and surrounding the tumor. This suggests a low grade primary glial neoplasm. Pathology confirmed this tumor to be a DNET.

Case 8: DNET tumor

A 16-year-old boy presented with seizures and was found to have a contrast enhancing mass at the left temporo-occipital lobe (Fig. 8). Susceptibility-weighted imaging (SWI) demonstrated internal hemorrhage within the mass. DTI deomstrated central reduced diffusion and displacement (rather than interruption) of the surrounding axon bundles. Prior to DTI, the differential diagnosis based upon conventional MR imaging would suggest primary glial neoplasm. Displacement, rather than disruption, of the fiber bundles at DTI is suggestive of lower grade neoplasm, which was confirmed at pathology to be a dysembryoplastic neuroepithelial (DNET) tumor. DNETs are pathologically benign cortical lesions that often arise in the temporal lobe. They usually are found in children and young adults with seizures that tend to become refractory to medical treatment. These lesions have many different imaging characteristics [Cruz et al., 2006; Koeller et al., 2006].

Case 9: Corpus callosum epidermoid cyst

A 46-year-old female presented to the emergency room with dizziness, fatigue, and nausea. MRI demonstrated a 4 cm mass mass arising from the posterior body of the corpus callosum. The mass was lobulated and had a heterogeneous appearance, decreased signal on T1, increased signal on T2, increased signal on diffusion-weighted imaging (DWI) and suppression of signal on the DarkFluid sequence. There was minimal post contrast enhancement of the mass. These characteristics are typical of an epidermoid cyst. DTI shows that the corpus callosum tracts are splayed superiorly, anteriorly and posteriorly with respect to the mass. The splenium is not involved (Fig. 9). The DTI findings are features of low grade lesions. Epidermoid cysts are benign slow-growing tumors which contain keratin, cellular debris and cholesterol, and lined with stratified squamous epithelium. Epidermoid cysts are most commonly located in the cerebellopontine angle cistern and the parasellar regions. Most are asymptomatic but may occasionally result in mass effect, cranial neuropathy, or seizure [Osborn et al., 2006]. Here we report a case of an epidermoid cyst that involves the body of the corpus callosum which is an unusual location.

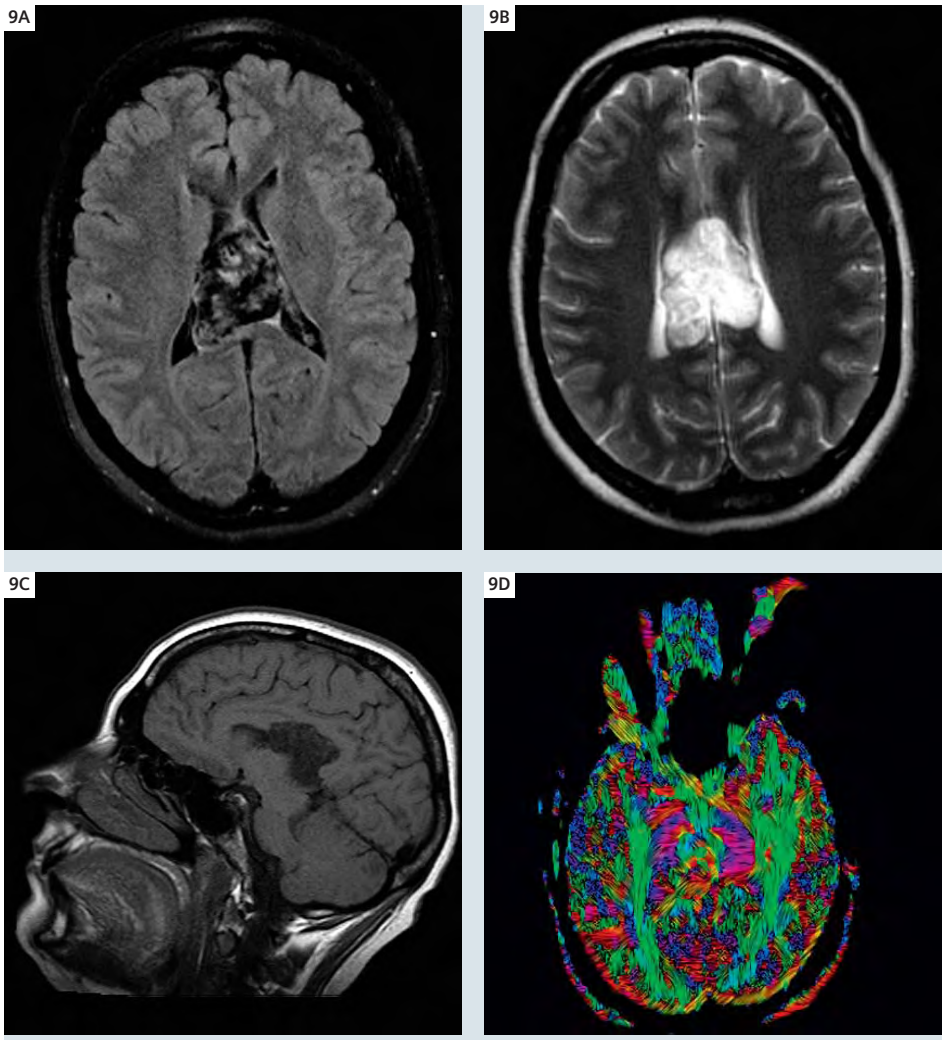

9 Corpus callosum epidermoid cyst. MR examinations were performed at 1.5T MAGNETOM Symphony, A Tim System: **(A)**, **(B)**, **(C)** are DarkFluid T2-weighted TSE, T2-weighted BLADE, and T1-weighted spin echo images respectively, demonstrating the mass associated with the posterior body of corpus callosum.

Continued on page 84

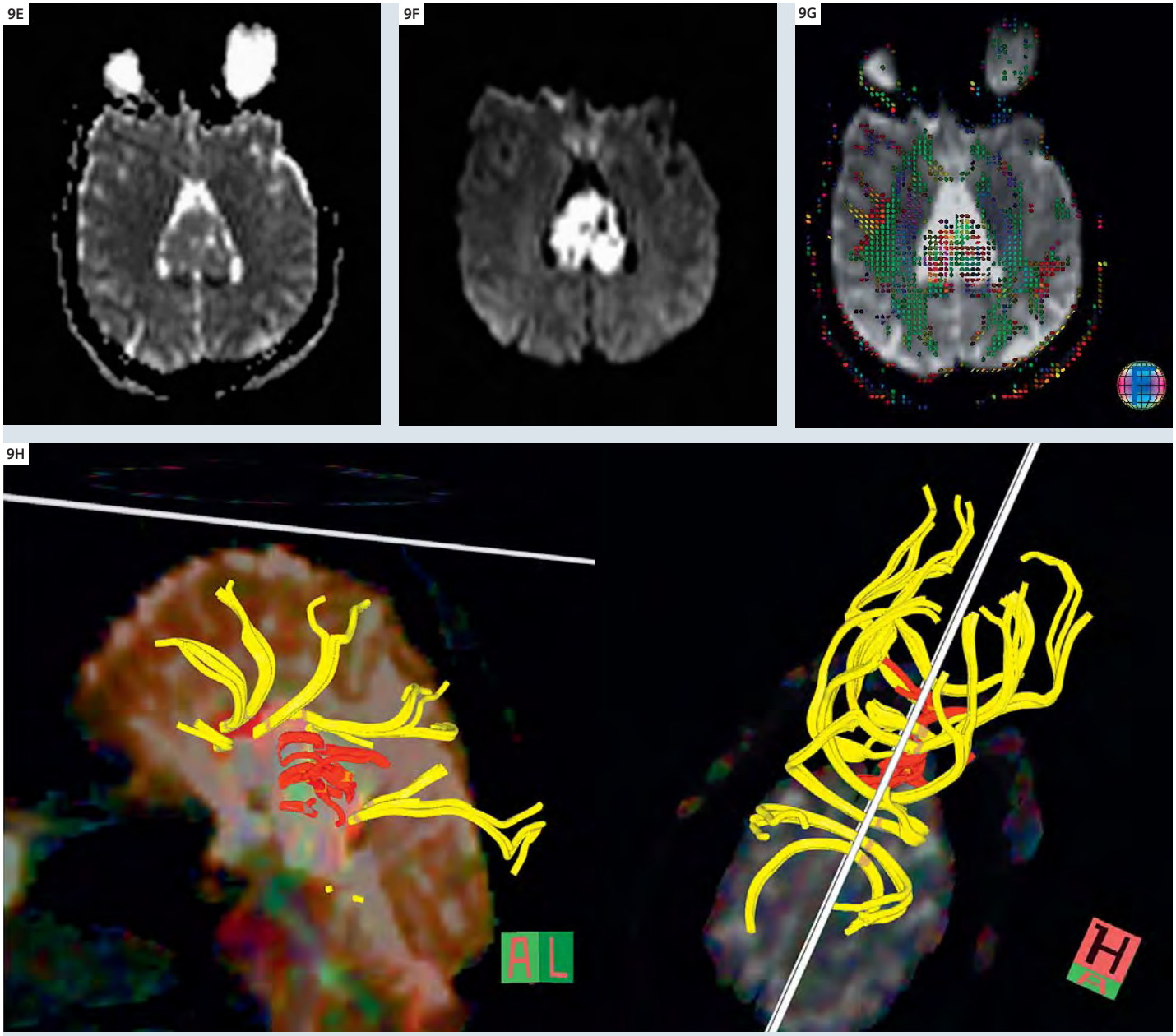

9 Corpus callosum epidermoid cyst **(D)**, **(E)**, **(F)**, **(G)** are the texture diffusion, ADC map, trace-weighted, and aligned tensor and anatomy still showing anisotropic diffusion surrounding the mass. **(H)** Tractography shows intact fibers of the corpus callosum (yellow) displaced superiorly above the mass (red). In this case, tractography proved useful for presurgical planning.

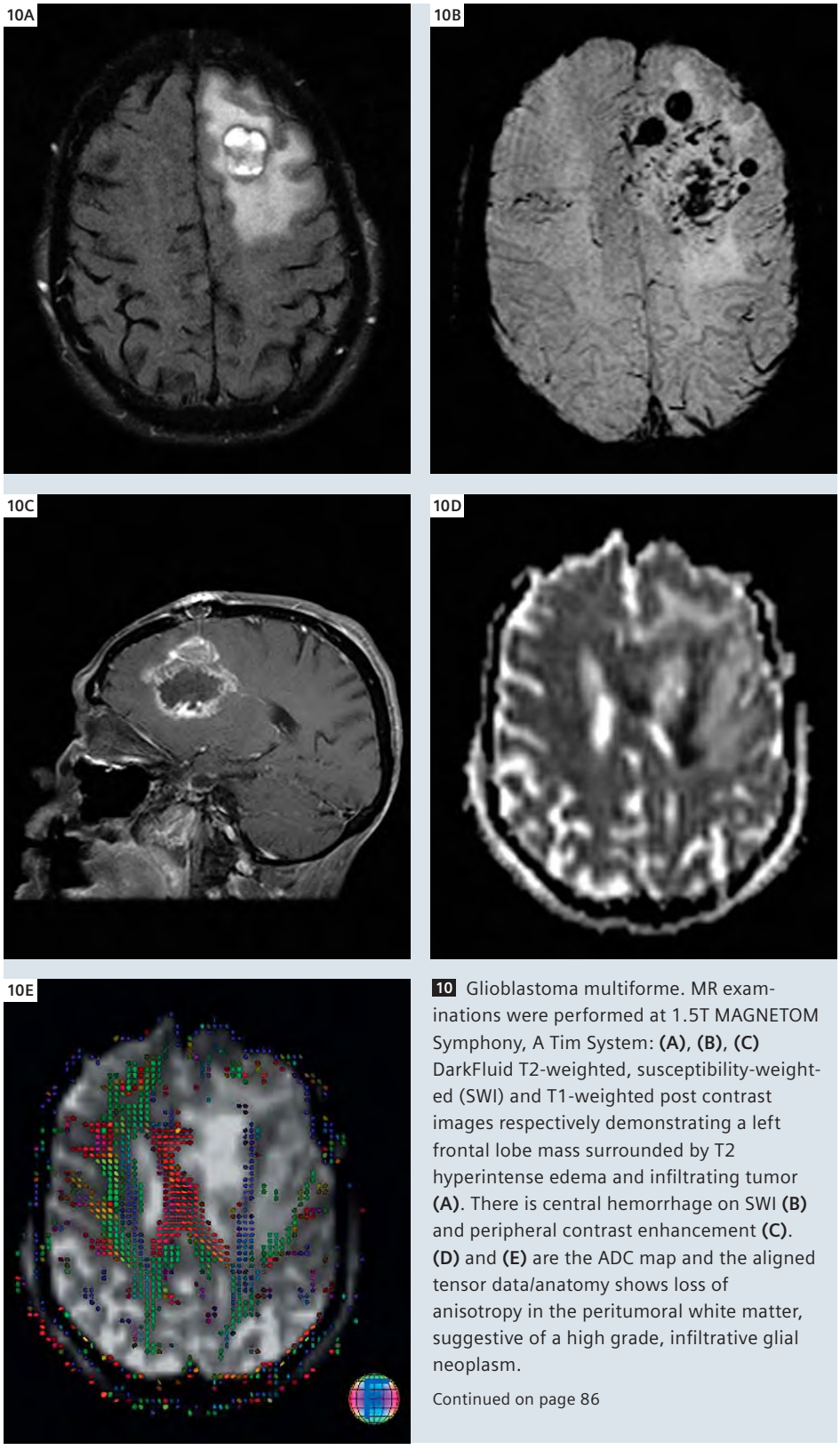

10 Glioblastoma multiforme. MR examinations were performed at 1.5T MAGNETOM Symphony, A Tim System: **(A)**, **(B)**, **(C)** DarkFluid T2-weighted, susceptibility-weighted (SWI) and T1-weighted post contrast images respectively demonstrating a left frontal lobe mass surrounded by T2 hyperintense edema and infiltrating tumor **(A)**. There is central hemorrhage on SWI **(B)** and peripheral contrast enhancement **(C)**. **(D)** and **(E)** are the ADC map and the aligned tensor data/anatomy shows loss of anisotropy in the peritumoral white matter, suggestive of a high grade, infiltrative glial neoplasm.

Continued on page 86

Case 10: Glioblastoma multiforme (GBM)

An 83-year-old woman was admitted with right limb weakness. MRI demonstrated a T2 hyperintense, hemorrhagic, contrast enhancing mass of the left frontal lobe. DTI shows disruption, rather than displacement, of left frontal white matter tracts, suggestive of a high grade glial neoplasm (Fig. 10). Biopsy confirmed the diagnosis of glioblastoma multiforme (GBM). Gliomas of astrocytic origin (astrocytomas) are classified into four grades pilocytic astrocytoma (grade I), astrocytoma (grade II), anaplastic astrocytoma (grade III) and glioblastoma multiforme (GMB) (grade IV), with different biological behaviour and degree of malignancy. Glioblastoma (GBM), the most common primary intracranial malignancy, is a morphologically diverse neoplasm with poor prognosis despite multimodality therapy [Roberts et al., 2005].

Conclusion

We have developed a fast, high resolution DTI protocol for whole brain DTI for implementation in routine clinical practice. Using standard Siemens DTI software at the scanner and standard post-processing, we routinely obtain 2 mm (3T) or 2.5 mm (1.5T) isotropic DTI with 25 b-values for all brain MRIs performed on Tim systems at Washington University. This adds less than 5 minutes to the brain MRI protocol. Post-processing for FA is performed inline at the scanner and is evaluated for all patients. Additional parameter maps and tractography for selected cases is performed with an additional 5–20 minutes of post-processing. The DTI is of high quality, and is obtained with additional averages (up to 10 to 20 minutes of total scanning time) for subjects involved in research studies. All of the cases presented in this review were identified during the course of routine clinical practice in a one month interval. On a daily basis, we are discovering new utility for DTI in our practice, with direct impact on current patient care.

10F

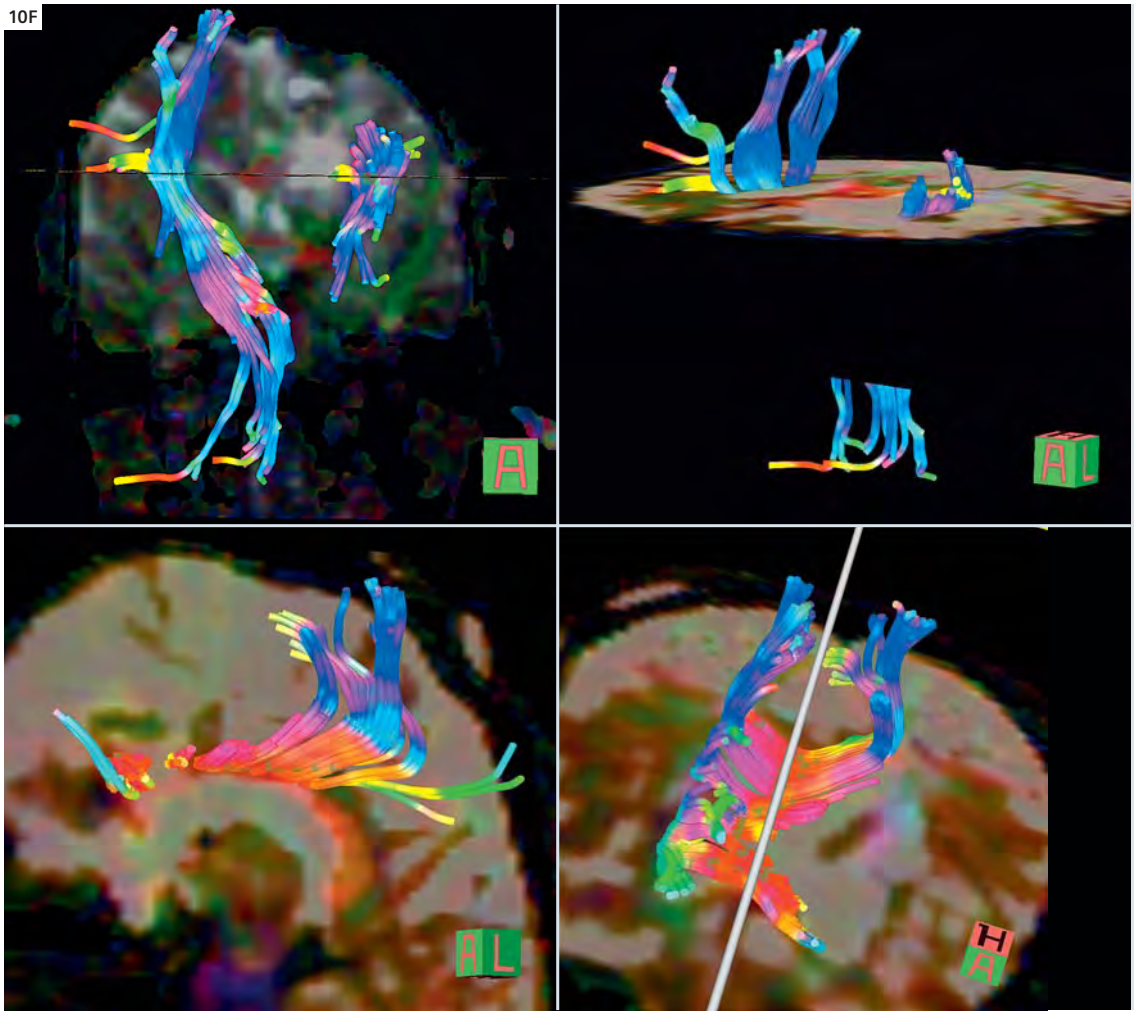

10 (F) Tractography images show the interrupted fibers around the tumor as would be expected for a high grade GBM (in contrast to the intact fibers around the low grademasses in figures 8 and 9). GBM was confirmed at pathology.

References

1 Alexander AL, Lee JE, Lazar M, Field AS.Diffusion tensor Imaging of the Brain. Neuroptherapeutics; 2007 July; 4:316-329.

2 Cruz LC Jr, Sorensen AG. Diffusion tensor magnetic resonance imaging of brain tumors. Magnetic Resonance Imaging Clinic North America. 2006 May; 14(2):183-202.

3 Doelken et al. Differentiation of cytotoxic and vasogenic edema in a patient with reversible posterior leukoencephalopathy syndrome using diffusion-weighted MRI. Diagn Interv Radiol 2007; 13: 125-128.

4 Eriksson S, Rugg-Gunn FJ, Symms MR, Barker GJ, Duncan JS. Diffusion tensor imaging in patients with epilepsy and malformations of cortical development. Brain 124: 617-626. 2001.

5 Folkerth RD. Periventricular Leukomalacia: Overview and Recent Findings. Pediatric and Developmental Pathology 2006;9; p3-13.

6 Inglese et al. Magnetization Transfer and Diffusion Tensor MR Imaging of Acute Disseminated Encephalomyelitis. AJNR 2002; 23; 267-272).

7 Koeller et al. Dysembryoplastic neuroepithelial tumors: MR appearance. AJNR 1992 Sep-Oct;13(5): 1319-25.

8 Krupp et al. Consensus definitions proposed for pediatric multiple sclerosis and related disorders. Neurology 2007; 68 (suppl 2): S7-12.

9 Melhem, ER, Mori, S, Mukundan, G, Kraut, M, Pomper, MG, van Zijl, PC

10 Diffusion Tensor MR Imaging of the Brain and White Matter Tractography, Am. J. Roentgenol. 2002 178: 3-16.

11 Min et al. Reversible Posterior Leukoencephalopathy in Connective Tissue Diseases. Semin Arthritis Rheum 2006: 35: 388-395.

12 Mukherjee P, McKinstry RC. Reversible posterior leukoencephalopathy syndrome: Evaluation with diffusion tensor imaging. Radiology. 2001 Jun;219(3):756-65.

13 Nagae LM. Diffusion Tensor Imaging in Children with Periventricular Leukomalacia: Variability of Injuries to White Matter Tacts. AJNR; 28; 1213-22, 2006.

14 Osborn et al. Intracranial Cysts: Radiologic-Pathologic Correlation and Imaging Approach. Radiology; 2006; vol 239; No. 3. p652-664.

15 Paul, LK et al. Agenesis of the corpus callosum: genetic, developmental and functional aspects of connectivity. Nature Reviews Neuroscience. 2007 April, vol 8, p287-299

16 Polizzi A, Pavone, P, Iannetti, P, Manfre, L, and Ruggieri, M. Septo-optic dysplasia complex: A heterogenous malformation syndrome. Pediatric Neurology Vol 34, No. 1, 2006.

17 Roberts TP, Liu F, et al. Fiber density index correlates with reduced fractional anisotropy in white matter of patients with glioblastoma. AJNR Am J Neuroradiol. 2005 Oct;26(9):2183-6.

18 Schoth, Felix, Krings, Timo. Diffusion-tensor imaging in septo-optic dysplasia. Neuroradiology, Vol 46, No 9, Sept 2004.

19 Song SK, Sun SW, Ramsbottom MJ, Chang C, Russell J, Cross AH. Dysmyelination revealed through MRI as increased radial (but unchanged axial) diffusion of water. Neuroimage. Nov 2002;17(3):1429-1436.

20 Stejskal EO, Tanner JE. Spin diffusion measurements: spin echoes in the presence of a time-dependent field gradient. J Chem Phys 1965;42:288 -292.

21 Tanaka et al. Genetics of brain development and malformation syndromes. Current Opinion in Pediatrics 2000, 12: 523-528.

22 Tovar-Moll F, Moll G, de Oliveira-Souza R, Bramati I, Andreiuolo PA, Lent R Neuroplasticity in Human Callosal Dysgenesis: A Diffusion Tensor Imaging Study, Cerebral Cortex Advance Access published on March 1, 2007, DOI 10.1093/cercor/bhj178. Cereb. Cortex 17: 531-541.

23 Trivedi R, Gupta RK, el al. Diffusion tensor imaging in polymicrogyria: a report of three cases. Neuroradiology. 2006 Jun; 48(6): 422-7.

24 Ward P, Counsell S, et al. Reduced fractional anisotropy on diffusion tensor magnetic resonance imaging after hypoxic-ischemic encephalopathy. Pediatrics. 2006 Apr;117(4):e619-30. Epub 2006 Mar 1.